MECHANIKA TEORETYCZNA
I STOSOWANA
Journal of Theoretical
and Applied Mechanics
1, 31, 1993

INFLUENCE OF THE RECTANGULAR PARALLELEPIPED INCLUSION ON TRANSIENT THERMAL STRESSES

ZBIGNIEW ORŁOŚ

GRZEGORZ GALIN

Military Technical Academy, Warsaw

An experimental investigation of transient thermal stresses that appear around the rectangular parallelepiped inclusion in the photoelastic plate made of Araldite B is described. The inclusion was made of aluminium – alloy plate. The effect of thermal load on the upper surface of plate was experimentally studied by means of photothermoelasticity. The results of experimental investigations have been compared with the results of theoretical investigations and numerical computations in terms of the computational FEM model.

1. Introduction

In this paper we shall consider the nature and magnitude of transient thermal stresses in the plate with the rectangular parallelepiped inclusion. The material used for the model of plate was Araldite B. The thermal stresses in the model were measured photoelastically. To simplify photothermoelastic studies under transient conditions, the technique of cooling by using powdered dry ice has been adopted, Orłoś and Galin (1992).

2. Experimental procedure

The geometry of the model made of Araldite B photoelastic material is shown in Fig.1[1]. The temperature dependent mechanical, thermal and photoelastic properties of the material were measured before the tests. Over the range of temperature from 200 K to 290 K the photoelastic figure of merit $Q_t = 19.3$ fringe/mK remained nearly constant.

[1]see the end of the paper

The rectangular parallelepiped inclusion was made of aluminium alloy and cemented into the photoelastic plate with epoxy adhesive. The mechanical and thermal properties of the materials used in this study are presented in Table 1.

Table 1. Mechanical and thermal properties of the materials at 293 K

Properties	Materials	
	Araldite B	Aluminium alloy
Shear modulus G [MPa]	1370	27000
Poisson's ratio ν	0.376	0.335
Thermal conductivity k $\left[\frac{W}{mK}\right]$	0.2	165
Specific heat c_p $\left[\frac{J}{kgK}\right]$	1050	673
Density ρ $\left[\frac{kg}{m^3}\right]$	1200	2650
Coefficient of expansion $[K^{-1}]$	6×10^{-5}	2.36×10^{-5}

The upper surface of the model was uniformly and suddenly cooled. The temperature in selected points was monitored with the aid fine copper-constantan thermocouples cemented into the model with epoxy resin.

Standard two-dimensional photoelastic techniques were used to determine isochromatics. The diffused light polariscope with 500 mm diameter field size was used. The continuous temperature measurement was performed, and simultaneously the photoelastic fringes were photographed and registred using television recording.

3. Results and conclusions

In the present experiment the Biot modulus is defined as

$$\mathrm{Bi} = \frac{hH}{k} \tag{3.1}$$

where

h – convective-heat-transfer coefficient,

k – thermal conductivity,

H – width of the plate.

The convective-heat-transfer coefficient was determined by measuring the temperature distribution over a special test beam made of Araldite B. The experiments on this beam resulted in an effective Biot modulus of 87.5 ± 10.

In Fig.2 is shown the dark – field isochromatic fringe pattern in the model at 120, 240 and 600 s after the thermal loading, respectively.

The transient thermal stresses in the two-dimensional theoretical model were determined using finite element analysis. A finite element mesh of the model is shown in Fig.3 in details.

The distributions of temperature difference $T - T_f$ (T – temperature of the model, $T_f = 200$ K) in the symmetrical section of the model are presented in Fig.4.

Comparison of the stress σ_x distributions over the section ($x = 0.5$ mm) close to the axis of symmetry of the model and the section ($x = 33.5$ mm) at 60 s is shown in Fig.5.

Comparison of the distributions of the stresses σ_x, σ_y and τ_{xy} over the section ($x = 32.5$ mm) in the plate with inclusion, and the stress σ_x in the plate without inclusion, at 600 s is shown in Fig.6.

Fig.7 shows the distributions of the stress σ_x in plate without inclusion and in plate with inclusion over the section ($x = 78$ mm) at 600 s.

The sharp corner of the inclusion edge causes the thermal-stress concentration in its vicinity.

To characterize this concetration the stress ratio φ_H is defined as

$$\varphi_H = \frac{\sigma_H}{\sigma_p} \tag{3.2}$$

where

σ_H – effective stress according to the Huber strain energy of distorsion theory,

$\sigma_p = -\frac{E\beta\Delta T}{1-\nu} = 33.71$ MPa,

$\Delta T = -93$ K – the maximal temperature difference $T - T_f$.

Fig.8 shows the distributions of the stress ratio φ_H close to the inclusion sharp edge corner, at 60, 120, 180 and 240 s.

The distribution of the effective stress σ_H in the plate is shown in Fig.9. The shape of the lines of equal effective stress σ_H is similar to the shape of both isochromatic fringes (Fig.2) and lines of equal maximum shear stress τ_{max} (Fig.10), respectively.

The main results obtained are summarized as follows.

The maximum thermal strains appear close to the inclusion sharp edge corner. Away from the inclusion edge the lines of equal effective stress and the lines of equal maximum shear stress are similar to the isochromatic fringes.

The influence of the inclusion on transient thermal stresses in the plate becomes negligible at the distance of approximately two lengths of the inclusion.

The presented two-dimensional computational FEM model has been employed to study the thermal plane stress distributions.

The existence of out-of-plane displacement restraints at the location of the thin photoelastic plate bondeding to the relatively rigid inclusion will induce trensverse

stress components and can cause the in-plane stresses to deviate from the plane-stress solution.

References

1. ORŁOŚ Z., GALIN G., 1992, *Investigation of Thermal Stresses in the I Beams with Circular Holes in the Web,* Mech.Teoret. i Stosow., 2, 30, 286-297
2. BLEJWAS T.E., LAUFFER W.D., TAUCHERT T.R., 1969, *Photothermoelastic Investigation in a Composite Model,* Experimental Mechanics, 478-480
3. RHINES W.J., WAJDA J.T., 1969, *The Effect of Out-of-plane Restraint on Plane-stress Solutions near Straight Boundaries,* Experimental Mechanics, 512-518
4. DURELLI A.J., 1970, *Photothermoelastic Investigation of Stresses in a Composite Model,* Experimental Mechanics, 216
5. KOKINI K., SMITH C.C., 1989, *Interfacial Transient Thermal Fracture of Adhesively Bonded Dissimilar Materials,* Experimental Mechanics, 29(3), 312-317

Wpływ inkluzji prostopadłościennej na niestacjonarne stany naprężenia

Streszczenie

W pracy opisano badania doświadczalne niestacjonarnych naprężeń i wpływ inkluzji prosopadłościennej w płytce wykonanej z materiału optycznie czynnego Araldite B na stany naprężeń cieplnych. Inkluzję wykonano ze stopu aluminiowego. Wpływ obciążenia cieplnego na górną powierzchnię płyty był badany doświadczalnie metoda termoelastooptyczną. Wyniki badań doświadczalnch były porównywane z wynikami rozważań teoretycznych oraz obliczeń numerycznych z wykorzystaniem metody elementów skończonych.

Manuscript received November 8, 1991; accepted for print September 28, 1992

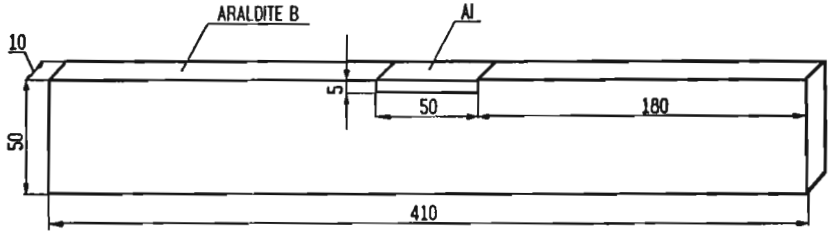

Fig. 1. Test-specimen with inclusion

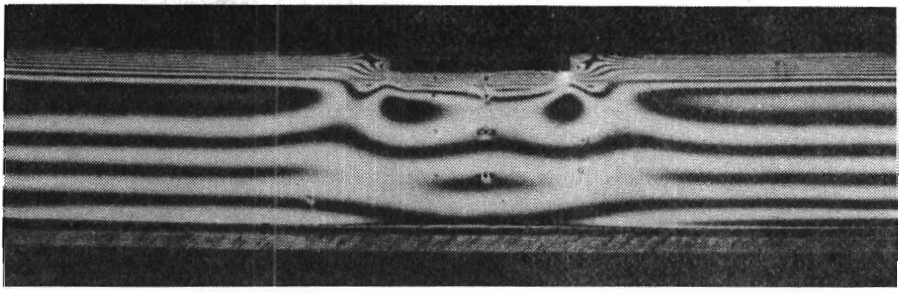

Fig. 2a

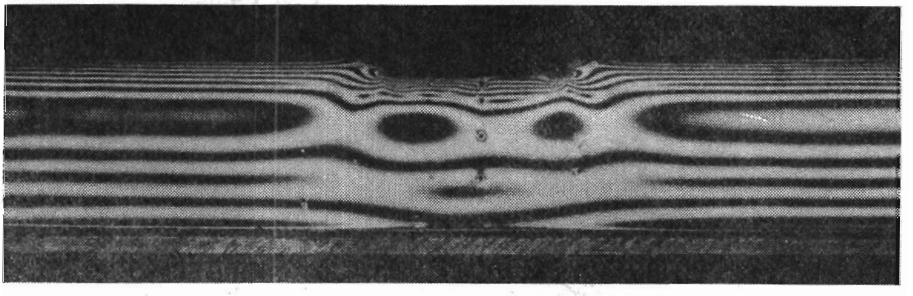

Fig. 2b

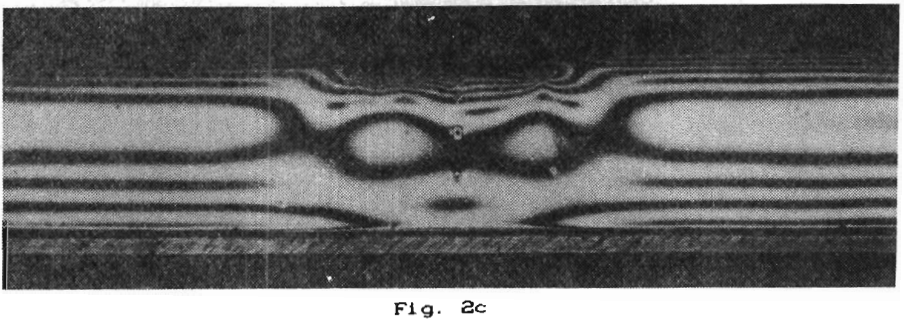

Fig. 2c

Fig. 2. Dark-field isochromatic fringe pattern in the model at the instants 120, 240 and 600 s

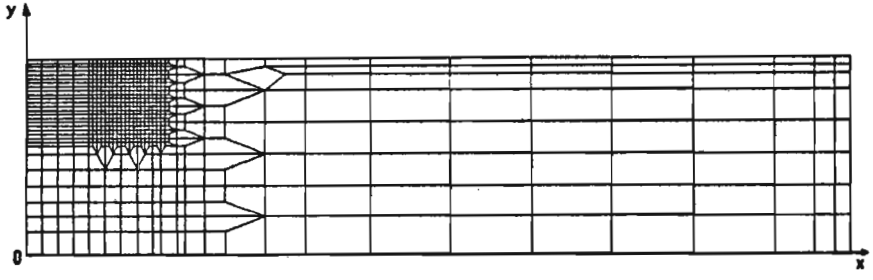

Fig. 3. The finite element mesh of the model

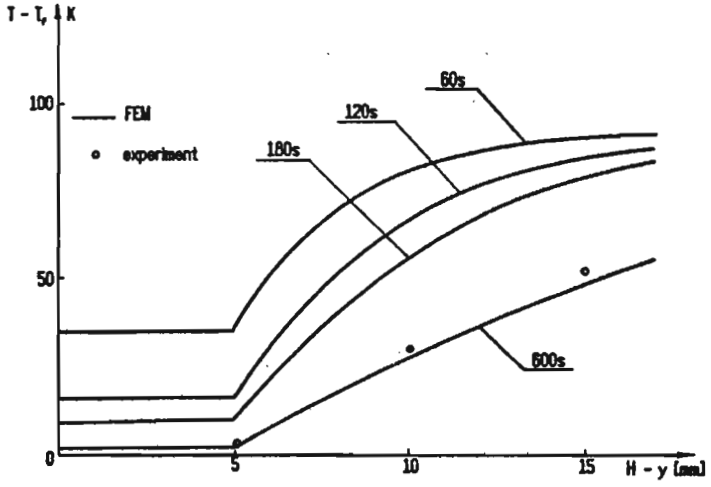

Fig. 4. The distributions of temperature difference $T - T_f$ over the symmetrical section of the model at the instants 60, 120, 180 and 600 s, respectively; $H = 50$ mm – width of the test-specimen

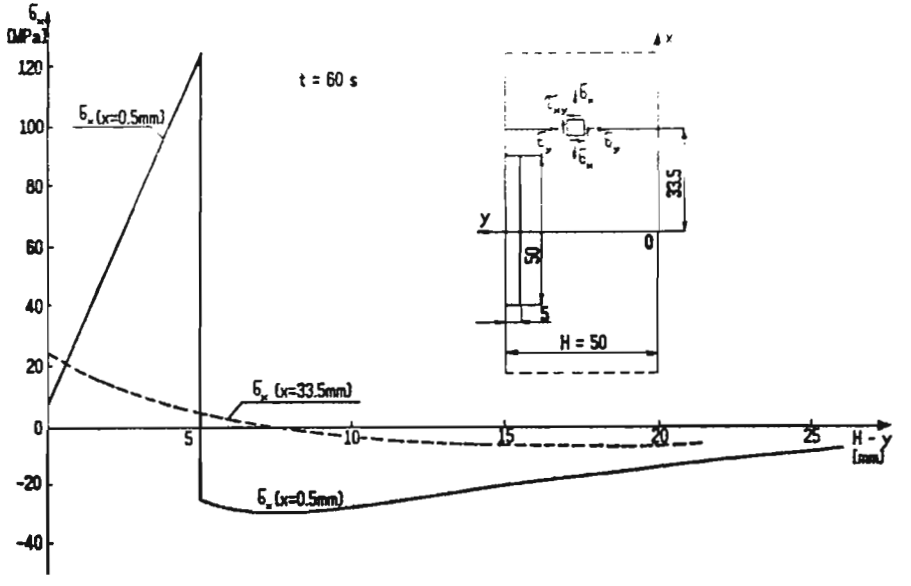

Fig. 5. Comparison between the distributions of stresses σ_x over the section ($x = 0.5$ mm) close to the axis of symmetry of the model and over the section ($x = 33.5$ mm)

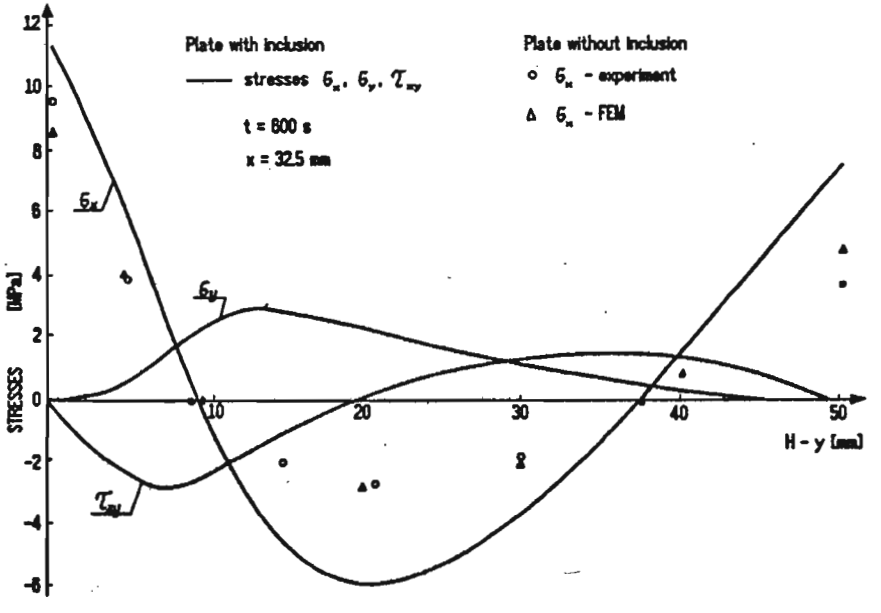

Fig. 6. Comparison between the distributions of the stresses σ_x, σ_y and τ_{xy} respectively in the plate with inclusion over the section ($x = 32.5$ mm) at the time 600 s, and the stresses σ_x in the plate without inclusion

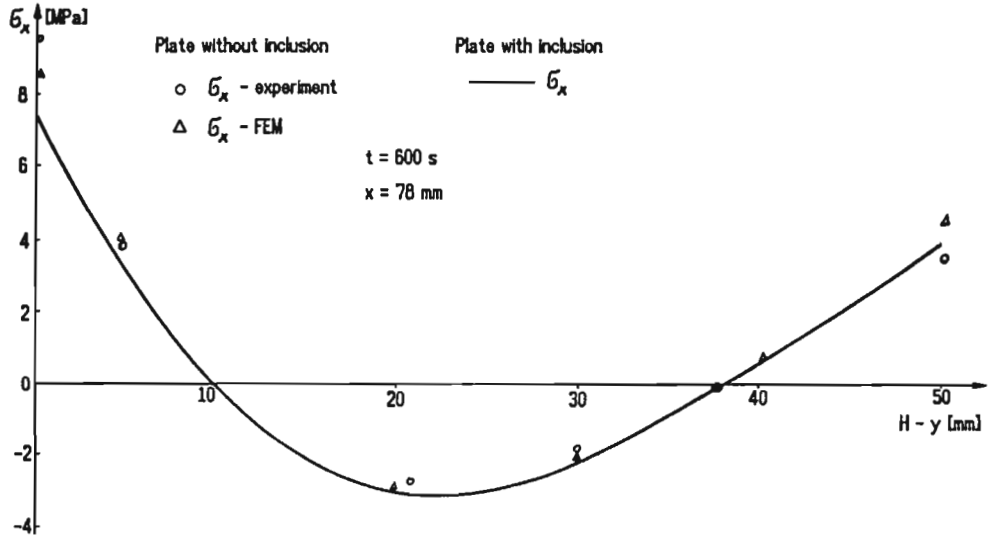

Fig. 7. The distributions of stress σ_x in the plate without inclusion and in the plate with inclusion over the section ($x = 78$ mm) at the instant 600 s

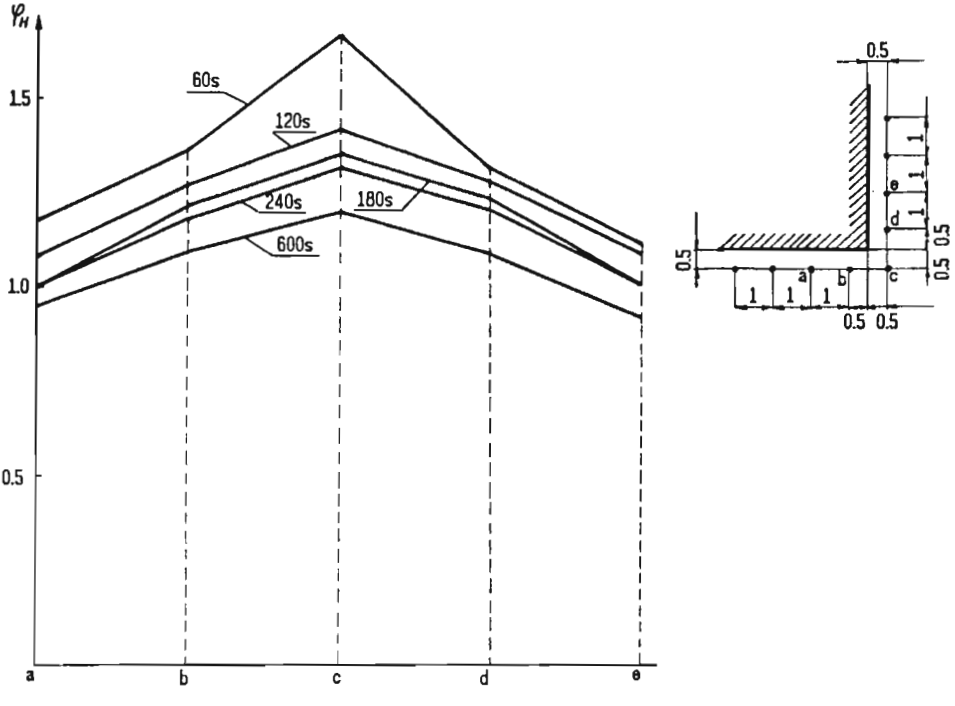

Fig. 8. The distributions of the stress ratio φ_H close to the inclusion edge, at the instant 60, 120, 180, 240 and 600 s, after the thermal loading, respectively

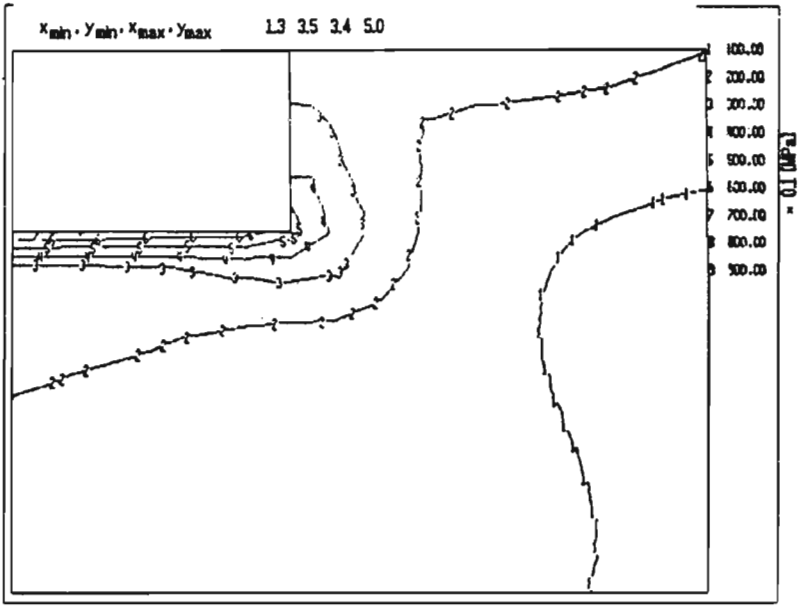

Fig. 9. The lines of equal effective stress σ_H at the instant 120 s

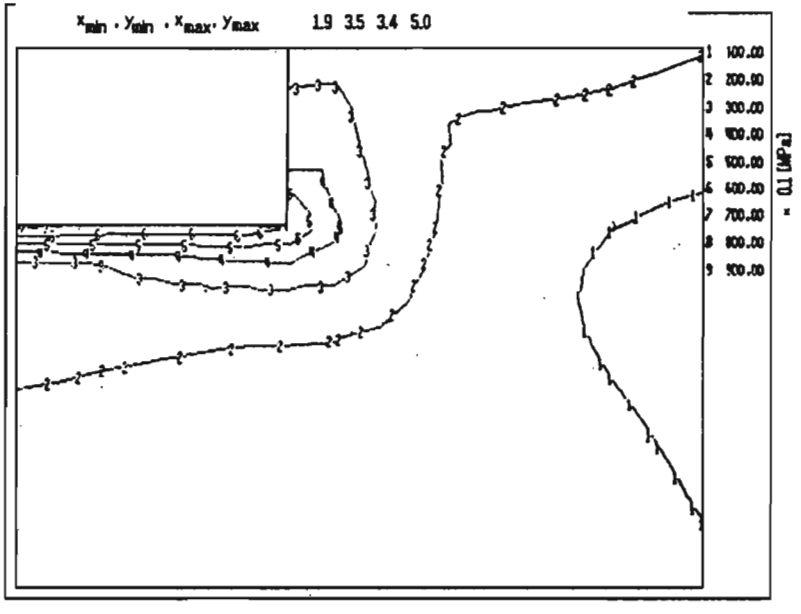

Fig. 10. The lines of equal difference of principal stresses $\sigma_1 - \sigma_2$ at the time 120 s